Inorg. Chem. **2002**, *41*, 1615–1624

Single- and Double-Cubane Clusters in the Multiple Oxidation States $[VFe_3S_4]^{3+,2+,1+}$

Christina Hauser,[†] Eckhard Bill,[‡] and R. H. Holm*[,†]

Department of Chemistry and Chemical Biology, Harvard University, Cambridge, Massachusetts 02138, and the Max-Planck-Institut für Strahlenchemie, D-45413 Mülheim an der Ruhr, Germany

Received September 27, 2001

A new series of cubane-type $[VFe_3S_4]^z$ clusters ($z = 1+, 2+, 3+$) has been prepared as possible precursor species for clusters related to those present in vanadium-containing nitrogenase. Treatment of $[(HBpz_3)VFe_3S_4Cl_3]^{2-}$ (**2**, $z = 2+$), protected from further reaction at the vanadium site by the tris(pyrazolyl)hydroborate ligand, with ferrocenium ion affords the oxidized cluster $[(HBpz_3)VFe_3S_4Cl_3]^{1-}$ (**3**, $z = 3+$). Reaction of **2** with Et_3P results in chloride substitution to give $[(HBpz_3)VFe_3S_4(PEt_3)_3]^{1+}$ (**4**, $z = 2+$). Reaction of **4** with cobaltocene reduced the cluster with formation of the edge-bridged double-cubane $[(HBpz_3)_2V_2Fe_6S_8(PEt_3)_4]$ (**5**, $z = 1+, 1+$), which with excess chloride underwent ligand substitution to afford $[(HBpz_3)_2V_2Fe_6S_8Cl_4]^{4-}$ (**6**, $z = 1+, 1+$). X-ray structures of (Me_4N)[**3**], [**4**](PF_6), **5**, and $(Et_4N)_4$[**6**]·2MeCN are described. Cluster **5** is isostructural with previously reported $[(Cl_4cat)_2(Et_3P)_2Mo_2Fe_6S_8(PEt_3)_4]$ and contains two VFe_3S_4 cubanes connected across edges by a Fe_2S_2 rhomb in which the bridging Fe-S distances are shorter than intracubane Fe–S distances. Mössbauer (**2**–**5**), magnetic (**2**–**5**), and EPR (**2**, **4**) data are reported and demonstrate an $S = 3/2$ ground state for **2** and **4** and a diamagnetic ground state for **3**. Analysis of ^{57}Fe isomer shifts based on an empirical correlation between shift and oxidation state and appropriate reference shifts results in two conclusions. (i) The oxidation **2** → **3** + e^- results in a change in electron density localized largely or completely on the Fe_3 subcluster and associated sulfur atoms. (ii) The most appropriate charge distributions are $[V^{3+}Fe^{3+}Fe^{2+}{}_2S_4]^{2+}$ ($Fe^{2.33+}$) for **1**, **2**, and **4** and $[V^{3+}Fe^{3+}{}_2Fe^{2+}S_4]^{3+}$ ($Fe^{2.67+}$) for **3** and $[V_2Fe_6S_8(SEt)_9]^{3+}$. Conclusion i applies to every MFe_3S_4 cubane-type cluster thus far examined in different redox states at parity of cluster ligation. The formalistic charge distributions are regarded as the best current approximations to electron distributions in these delocalized species. The isomer shifts require that iron atoms are mixed-valence in each cluster.

Introduction

The structures of the cofactor and P clusters of nitrogenase are now well established in several oxidation states by protein crystallography.[1−3] Elsewhere, we have pointed out that heterometal cubane-type clusters with cores $[MFe_3S_4]^z$ are potentially useful precursors in attaining synthetic representations of the iron−molybdenum (FeMoco) and iron−vanadium (FeVco) cofactors of nitrogenase.[4] The synthetic clusters and cofactors have in common cuboidal MFe_3S_3 substructures. Further, we have shown that the reduced cores $[MoFe_3S_4]^{2+}$ are effective entities in the formation of clusters whose fragments are topological analogues of the P^N cluster of nitrogenase.[5,6] Vanadium EXAFS results[7−11] and other

* Author to whom correspondence should be addressed. E-mail: holm@chemistry.harvard.edu.
[†] Harvard University.
[‡] Max-Planck-Institut.

(1) Chan, M. K.; Kim, J.; Rees, D. C. *Science* **1993**, *260*, 792−794.
(2) Peters, J. W.; Stowell, M. H. B.; Soltis, S. M.; Finnegan, M. G.; Johnson, M. K.; Rees, D. C. *Biochemistry* **1997**, *36*, 1181−1187.
(3) Mayer, S. M.; Lawson, D. M.; Gormal, C. A.; Roe, S. M.; Smith, B. E. *J. Mol. Biol.* **1999**, *292*, 871−891.
(4) Huang, J.; Mukerjee, S.; Segal, B. M.; Akashi, H.; Zhou, J.; Holm, R. H. *J. Am. Chem. Soc.* **1997**, *119*, 8662−8674.
(5) Osterloh, F.; Sanakis, Y.; Staples, R. J.; Münck, E.; Holm, R. H. *Angew. Chem., Int. Ed.* **1999**, *38*, 2066−2070.
(6) Osterloh, F.; Achim, C.; Holm, R. H. *Inorg. Chem.* **2001**, *40*, 224−232.
(7) Arber, J. M.; Dobson, B. R.; Eady, R. R.; Stevens, P.; Hasnain, S. S.; Garner, C. D.; Smith, B. E. *Nature* **1987**, *325*, 372−374.
(8) George, G. N.; Coyle, C. L.; Hales, B. J.; Cramer, S. P. *J. Am. Chem. Soc.* **1987**, *110*, 4057−4059.
(9) Arber, J. M.; Dobson, B. R.; Eady, R. R.; Hasnain, S. S.; Garner, C. D.; Matsushita, T.; Nomura, M.; Smith, B. E. *Biochem. J.* **1989**, *258*, 733−737.

10.1021/ic011011b CCC: $22.00
Published on Web 02/21/2002

considerations[10,11] point to a VS_3O_2N coordination unit analogous to that in FeMoco, implicating cluster sulfide, homocitrate hydroxyl and carboxylate, and histidyl imidazole ligands. The synthesis and structural characterization of cubane-type VFe_3S_4 clusters have provided species with vanadium coordination units similar to that in FeVco.[4,12−15]

The large majority of our research related to nitrogenase clusters has involved $[MoFe_3S_4]^{2+,3+}$ species. We have commenced a parallel examination of VFe_3S_4 clusters as precursors to higher-nuclearity species (e.g., $V_2Fe_6S_{7-9}$, VFe_7S_9) that are compositional and/or topological analogues of enzyme clusters. Issues that immediately arise include the scope of synthetically accessible core oxidation states $[VFe_3S_4]^z$ and reactions leading to the formation of higher-nuclearity clusters from single cubanes in one or more oxidation states. The first VFe_3S_4 clusters prepared, typified by $[(DMF)_3VFe_3S_4Cl_3]^{1-}$,[12] illustrate the stability of $[VFe_3S_4]^{2+}$, the state formed in cluster self-assembly and retained in ligand substitution reactions. Thereafter, voltammetry of the $[VFe_3S_4]^{2+}$ cluster $[(HBpz_3)VFe_3S_4(LS_3)]^{2-}$ revealed reversible conversion among the three oxidation states $[VFe_3S_4]^{3+,2+,1+}$,[15] and subsequent synthetic work afforded the $[VFe_3S_4]^{3+}$ oxidation level in the isolated double-cubane cluster $[V_2Fe_6S_8(SEt)_9]^{3-}$ [16] and in $[VFe_3S_4(Et_2dtc)_4]^{1-}$.[17] (Ligand abbreviations are defined in Chart 1.) The present investigation was undertaken to obtain a related set of clusters in different oxidation states, define certain ground-state electronic properties of these states, and determine if higher-nuclearity clusters can be derived from single-cubane $[VFe_3S_4]^z$ species.

Experimental Section

Preparation of Compounds. All operations were carried out at room temperature using either Schlenk or standard glovebox techniques. Solvents were dried by distillation from sodium/benzophenone (diethyl ether, tetrahydrofuran, and hexanes) or CaH_2 (acetonitrile) and degassed thoroughly prior to use. Triethylphosphine and $[Cp_2Fe](PF_6)$ were obtained from Aldrich. Potassium tris(pyrazolyl)hydroborate was prepared as described.[18] The published procedure for $(Me_4N)_2[(HBpz_3)VFe_3S_4Cl_3]\cdot 2MeCN$[14] was slightly modified by using Me_4NCl instead of Me_4NBr for cluster crystallization to avoid the possibility of mixed halide ligation. In the following preparations, solvent removal and drying steps were performed in vacuo.

$(Me_4N)[(HBpz_3)VFe_3S_4Cl_3]$. $(Me_4N)_2[(HBpz_3)VFe_3S_4Cl_3]\cdot 2MeCN$ (150 mg, 0.175 mmol) was dissolved in 1 mL of acetonitrile to give a dark brown solution. A deep blue solution of $[Cp_2Fe](PF_6)$ (65.2 mg, 0.197 mmol) in 0.5 mL of acetonitrile was added. The reaction mixture was stirred for 30 min during which a colorless solid precipitated. The green-black solution was filtered through Celite, and the filtrate was taken to dryness. The remaining black residue was washed with hexane (2×2.5 mL) and dried, and the solid was dissolved in 1 mL of acetonitrile. The black-green solution was filtered through Celite and layered with 2.5 mL of ether. A colorless precipitate of Me_4NPF_6 was removed by filtration. On standing for 2 days, the product separated as 99.4 mg (77%) of black crystalline product. IR (KBr): ν_{BH} 2453 cm^{-1}. ^{1}H NMR (CD_3CN, anion): δ 6.80, 9.33, 10.92 (CH). Anal. Calcd for $C_{13}H_{22}BCl_3Fe_3N_7S_4V$: C, 21.09; H, 3.00; Cl, 14.37; Fe, 22.63; N, 13.24; S, 17.32; V, 6.88. Found: C, 21.19; H, 3.01; Cl, 14.34, Fe, 22.57; N, 13.32; S, 17.19; V, 7.06.

$[(HBpz_3)VFe_3S_4(PEt_3)_3](PF_6)$. $(Me_4N)_2[(HBpz_3)VFe_3S_4Cl_3]\cdot 2MeCN$ (210 mg, 0.246 mmol) was dissolved in 5 mL of acetonitrile, and PEt_3 (180 μL, 1.22 mmol) was added to the brown-black solution. After the reaction mixture was stirred for 1 min, a suspension of $NaPF_6$ (205 mg, 1.22 mmol) in 2 mL of acetonitrile was added. Stirring was continued for 16 h during which black and colorless precipitates formed. Addition of ether and overnight storage afforded more solid and a nearly colorless solution. The solvents were decanted, and the remaining solid was dried. This material was extracted with dichloromethane, dissolving only the black solid. The brown-black extract was filtered through Celite. Slow diffusion of hexanes into the filtrate yielded the product as a black crystalline solid (128 mg, 49%). IR (KBr): ν_{BH} 2500 cm^{-1}. ^{1}H NMR (CD_3CN): δ 2.24 (PCH_2CH_3), 6.85 (CH), 10.69 (PCH_2CH_3), 13.37 (CH), 14.99 (CH). Anal. Calcd for $C_{27}H_{55}BF_6Fe_3N_6P_4S_4V$: C, 30.62; H, 5.23; Fe, 15.82; N, 7.93; P, 11.70; S, 12.11; V, 4.81. Found: C, 30.53; H, 5.18; Fe, 15.75; N, 7.99; P, 11.83; S, 12.06; V, 4.67

$[(HB(pz)_3)_2V_2Fe_6S_8(PEt_3)_4]$. $[(HBpz_3)VFe_3S_4Cl_3(PEt_3)_3](PF_6)$ (106 mg, 0.100 mmol) was dissolved in 2.5 mL of acetonitrile, and a solution of 19.7 mg (0.104 mmol) of Cp_2Co in 1 mL of acetonitrile was added. The reaction mixture was stirred for 1 min and filtered through Celite. The filtrate was allowed to stand overnight, during which the product separated as a black crystalline solid (73.9 mg, 93%). IR (KBr): ν_{BH} 2459 cm^{-1}. ^{1}H NMR ($CDCl_3$): δ 3.27 (PCH_2CH_3); 6.47, 13.6, 17.2 (CH); 19.0, 19.4 (PCH_2CH_3). Anal. Calcd for $C_{42}H_{80}B_2Fe_6N_{12}P_4S_8V_2$: C, 31.68; H, 5.06; Fe, 21.05; N, 10.56; P, 7.78; S, 16.11; V, 6.40. Found: C, 31.58; H, 5.00; Fe, 20.96; N, 10.61; P, 7.91; S, 15.97; V, 6.52.

$(Et_4N)_4[(HB(pz)_3)_2V_2Fe_6S_8Cl_4]$. $[(HBpz_3)_2V_2Fe_6S_8(PEt_3)_4]$ (55.2 mg, 0.035 mmol) was suspended in 3.5 mL of acetonitrile, and a solution of 116 mg (0.698 mmol) of Et_4NCl in 1.5 mL of acetonitrile was added, causing all the solid to dissolve. The green-brown mixture was stirred for 1 min and filtered through Celite. Slow diffusion of ether resulted in separation of the product as a black crystalline solid (46.3 mg, ~60%). IR (KBr): ν_{BH} 2480 cm^{-1}. ^{1}H NMR (DMSO-d_6, anion): δ 6.17, 13.2, 17.8 (CH). Analytical data suggest an ether tetrasolvate. Anal. Calcd for $C_{66}H_{140}B_2Cl_4Fe_6N_{16}O_4S_8V_2$: C, 38.12; H, 6.79; Cl, 6.82; Fe, 16.12; N, 10.78; S, 12.34; V, 4.90. Found: C, 37.85; H, 6.24; Cl, 7.35; Fe, 16.05; N, 12.07; S, 13.09; V, 5.04.

In the sections that follow, clusters are designated as in Chart 1.

X-ray Structure Determinations. Crystal structures were obtained for the four compounds in Table 1. Suitable crystals of (Me_4N)[**3**] were obtained by ether diffusion into an acetonitrile solution; [**4**](PF_6) by diffusion of hexanes into a dichloromethane solution; and $(Et_4N)_4$[**6**]·2MeCN by diffusion of THF into an acetonitrile solution. Crystals of **5** were isolated from the reaction mixture. Crystals were coated with oil and mounted on a Bruker

(10) Eady, R. R. *Chem. Rev.* **1996**, *96*, 3013−3030.
(11) Smith, B. E. *Adv. Inorg. Chem.* **1999**, *47*, 160−218.
(12) Kovacs, J. A.; Holm, R. H. *Inorg. Chem.* **1987**, *26*, 702−711.
(13) Kovacs, J. A.; Holm, R. H. *Inorg. Chem.* **1987**, *26*, 711−718.
(14) Malinak, S. M.; Demadis, K. D.; Coucouvanis, D. *J. Am. Chem. Soc.* **1995**, *117*, 3126−3133.
(15) Ciurli, S.; Holm, R. H. *Inorg. Chem.* **1989**, *28*, 1685−1690.
(16) Cen, W.; Lee, S. C.; Li, J.; MacDonnell, F. M.; Holm, R. H. *J. Am. Chem. Soc.* **1993**, *115*, 9515−9523.
(17) Deng, Y.; Liu, Q.; Chen, C.; Wang, Y.; Cai, Y.; Wu, D.; Kang, B.; Liao, D.; Cui, J. *Polyhedron* **2000**, *16*, 4121−4128.
(18) Trofimenko, S. *Inorg. Synth.* **1970**, *12*, 99−109.
(19) Palermo, R. E.; Singh, R.; Bashkin, J. K.; Holm, R. H. *J. Am. Chem. Soc.* **1984**, *106*, 2600−2612.

Table 1. Crystallographic Data[a]

	(Me_4N)[**3**]	[**4**](PF_6)	**5**	$(Et_4N)_4$[**6**]·2MeCN
formula	$C_{13}H_{22}BCl_3Fe_3N_7S_4V$	$C_{27}H_{55}BF_6Fe_3N_6P_4S_4V$	$C_{42}H_{80}B_2Fe_6N_{12}P_4S_8V_2$	$C_{54}H_{106}B_2Cl_4Fe_6N_{18}S_8V_2$
fw	740.27	1059.19	1592.14	1864.45
cryst syst	monoclinic	orthorhombic	monoclinic	monoclinic
space group	$P2_1/c$	$Pbca$	$P2_1/n$	$P2_1/n$
Z	4	8	2	2
a, Å	9.280(1)	21.060(1)	11.365(1)	14.429(2)
b, Å	27.548(3)	19.808(1)	25.114(1)	14.217(2)
c, Å	11.585(1)	21.114(1)	12.709(1)	19.412(3)
β, deg	112.978(2)		112.238(1)	94.212(2)
V, Å^3	2726.8(6)	8807.6(9)	3357.5(3)	3972(1)
d_{calcd}, g/cm^3	1.803	1.598	1.575	1.559
μ, mm^{-1}	2.514	1.564	1.907	1.680
T, K	213	213	213	213
2θ range, deg	3 → 45	3 → 56	3 → 45	4 → 47
GOF (F^2)	1.075	1.017	1.082	1.035
R_1[b], wR_2[c]	0.0513, 0.1361	0.0637, 0.1411	0.0556, 0.1366	0.0348, 0.0944

[a] Obtained with graphite-monochromated Mo Kα ($\lambda = 0.71073$ Å) radiation at 213 K. [b] $R_1 = \sum||F_o| - |F_c||/\sum|F_o|$. [c] $wR_2 = \{\sum[w(F_o^2 - F_c^2)^2]/\sum[w(F_o^2)^2]\}^{1/2}$.

Chart 1. Designation of Clusters[a,b]

$[(DMF)_3VFe_3S_4Cl_3]^{1-}$	**1**[12]
$[(HBpz_3)VFe_3S_4Cl_3]^{2-}$	**2**[14]
$[(HBpz_3)VFe_3S_4Cl_3]^{1-}$	**3**
$[(HBpz_3)VFe_3S_4(PEt_3)_3]^{1+}$	**4**
$[(HBpz_3)_2V_2Fe_6S_8(PEt_3)_4]$	**5**
$[(HBpz_3)_2V_2Fe_6S_8Cl_4]^{4-}$	**6**
$[(Cl_4cat)(MeCN)MoFe_3S_4Cl_3]^{2-}$	**7**[19]
$[(Cl_4cat)(MeCN)MoFe_3S_4(PR_3)_3]$	**8**[20]
$[(Cl_4cat)_2(Et_3P)_2Mo_2Fe_6S_8(PEt_3)_4]$	**9**[20,21]

[a] Ligands bound to the heterometal precede V or Mo. [b] Abbreviations: Cl_4cat = tetrachlorocatecholate(2-); edt = ethane-1,2-dithiolate(2-); Et_2dtc = *N*,*N*-diethyldithiocarbamate(1-); $HBpz_3$ = tris(pyrazolyl)hydroborate(1-); LS_3 = 1,3,5-tris((4,6-dimethyl-3-mercaptophenyl)thio)-2,4,6-tris(*p*-tolyl-thio)benzene(3-).

CCD area detector instrument operated by the SMART software package. Data collection and reduction and absorption corrections were performed as described elsewhere.[20] Space groups were identified on the basis of systematic absences by the program XPREP and by successful structure solution and refinement. The structures were solved by direct methods using the SHELXS-97 program suite and by full matrix least-squares on F^2 employing the SHELXL-97 program. Hydrogen atoms were placed in idealized positions, and displacement parameters were set at 1.2 times those of the attached aromatic carbon or boron atoms. Displacement parameters for hydrogen atoms bound to nonaromatic carbon atoms were set at 1.5 times those of the attached atoms. During the final cycles, all non-hydrogen atoms were refined anisotropically unless stated otherwise. For [**4**](PF_6), anion disorder was modeled in two orientations. Molecules of **5** lie on an inversion center; disorder of ethyl groups was modeled in two superimposed orientations of half-occupancy. All non-hydrogen atoms except the carbon atoms of the phosphine ligands were described anisotropically. Due to an inversion center in crystals of $(Et_4N)_4$[**6**]·2MeCN, the asymmetric unit contains one-half anion, two cations, and an acetonitrile solvate molecule. One of the cations is disordered and was modeled over two positions of equal occupancy. Crystal parameters and final agreement factors are collected in Table 1. (See Supporting Information paragraph.)

Other Physical Measurements. Infrared spectra of solid samples (KBr disk) were measured on a Nicolet Nexus 470 FT-IR spectrometer. ^{1}H NMR spectra were recorded with a Bruker AM 400N spectrometer. Cyclic voltammograms were obtained with a PAR model 263 potentiostat/galvanostat using a glassy carbon disk working electrode and 0.1 M $(Bu_4N)(PF_6)$ as a supporting electrolyte. Potentials are reported vs the saturated calomel electrode (SCE). Mössbauer data were recorded on an alternating constant-acceleration spectrometer; the minimum line width was 0.24 mm/s (full width at half-height). The sample temperature was maintained with either an Oxford Instruments Variox or Mössbauer−Spectromag cryostat. The latter is a split-pair superconducting magnet system for applied fields up to 8 T where the temperature of the sample can be varied over 1.5−250 K. Isomer shifts are quoted relative to iron metal at 300 K. Magnetic susceptibilities of powdered samples were recorded on a SQUID magnetometer (MPMS, Quantum Design) in the range of 2−295 K with an applied field of 1 T or at several fields with values sampled on a linear 1/T scale (multifield multitemperature measurements). Experimental susceptibility data were corrected for underlying diamagnetism with the use of Pascal's constants. Magnetic data were simulated by using the spin-Hamiltonian program JULIUS.

X-band EPR spectra were recorded on a Bruker ESP 300E spectrometer equipped with a helium flow cryostat (Oxford Instruments ESR 910), an NMR field probe (Bruker 035M), and a microwave frequency counter (HP5352B). Spin-Hamiltonian simulations of the EPR spectra were performed with a program developed from the $S = 5/2$ routines of Gaffney and Silverstone,[22] which specifically make use of the resonance-search procedure based on a Newton−Raphson algorithm described therein. Frequency- and angular-dependent contributions to the line widths were considered in the powder simulations. The line shape of the spin packets were either Lorentzian or Gaussian, derivative or absorption lines, depending on the type of spectra. The simulations are based on the spin-Hamiltonian below for the electronic ground-state spin multiplet, where S is the total spin multiplet and D and E/D are the usual axial and rhombic and zero-field parameters, respectively.

$$H = D[S_z^2 - S(S+1)/3 + (E/D)(S_x^2 - S_y^2)] + \mu_B \cdot \boldsymbol{B} \cdot g \cdot \boldsymbol{S}$$

Distributions of E/D (or alternatively D) were taken into account by summation of a series of powder spectra calculated at distinct

(20) Osterloh, F.; Segal, B. M.; Achim, C.; Holm, R. H. *Inorg. Chem.* **2000**, *39*, 980−989.

(21) Demadis, K. D.; Campana, C. F.; Coucouvanis, D. *J. Am. Chem. Soc.* **1995**, *117*, 7832−7833.

(22) Gaffney, B. J.; Silverstone, H. J. *Biol. Magn. Res.* **1993**, *13*, 1−57.

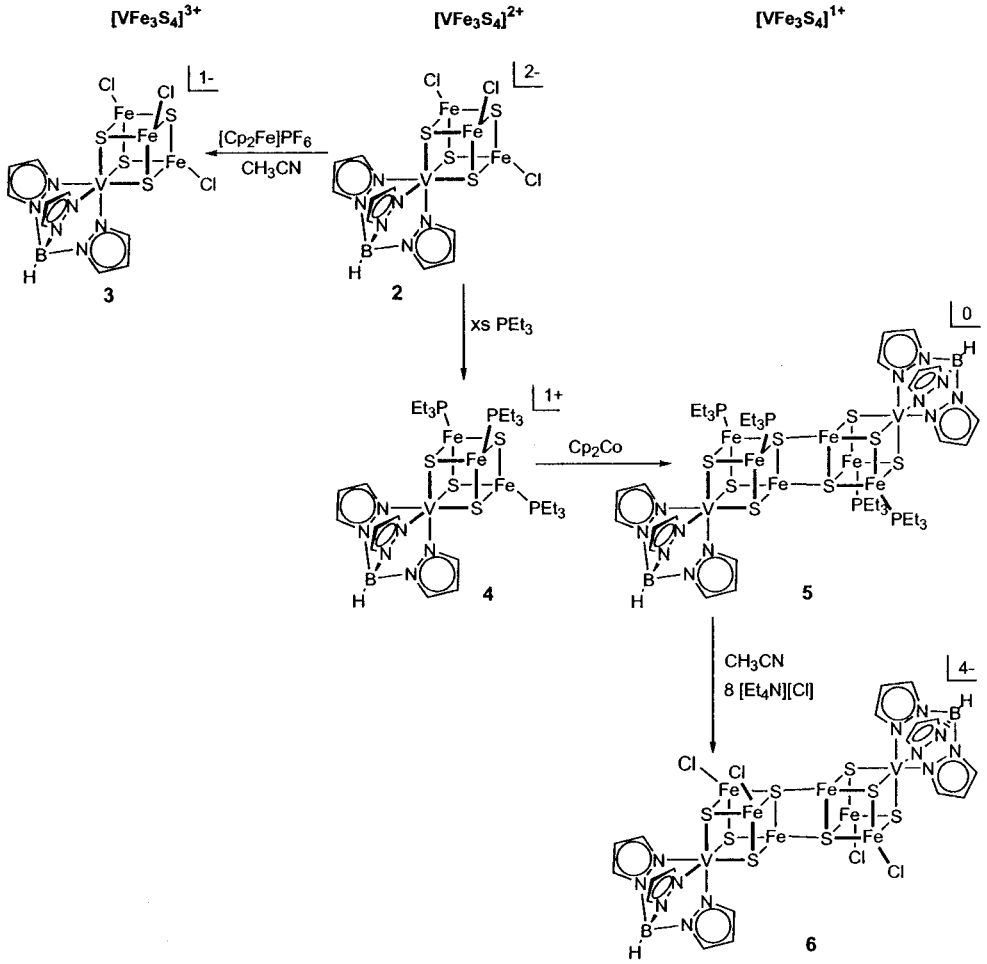

Figure 1. Scheme for the synthesis of single-cubanes **3** and **4** and edge-bridged double-cubanes **5** and **6** from precursor cluster **2**. Core oxidation levels are indicated.

values of that parameter with weight factors taken from the Gaussian distribution. The distributed parameter was equidistantly sampled in a range ±3 times the width of the Gaussian distribution, and usually 20 EPR spectra were superimposed in this procedure. The intrinsic width of the spin-packets (Gaussian line shape) was taken to be at least 10 mT (at $g = 2$).

Results and Discussion

Synthesis and Structures of Clusters. The synthetic scheme presented in Figure 1 originates with DMF solvate cluster **1** (not shown), which, as previously demonstrated,[14] undergoes ligand substitution at the vanadium site to afford **2**. The cluster $[(MeCN)_3VFe_3S_4Cl_3]^{1-}$ has recently been isolated and structurally characterized;[23] it is expected to have similar reactivity. The indicated structure of **2**, in which the vanadium site is blocked from further reaction, has been crystallographically established, but accurate metric features were not determined.[14] It serves as the precursor to clusters **3**−**6**, which were obtained as black solids. In acetonitrile, **2** exhibits a reversible one-electron oxidation at −0.11 V (ΔE_p = 90 mV) and an irreversible reduction at ca. −1.35 V ($i_{pc}/i_{pa} \gg 1$, 100 mV/s). It is readily oxidized by ferrocenium ion in acetonitrile to afford **3**, containing the $[VFe_3S_4]^{3+}$ core and isolated as the Me_4N^+ salt (77%). Treatment of **2** with 5 equiv of Et_3P effected complete substitution of chloride and the formation of **4**, which was obtained as the PF_6^- salt (49%). Previously, we have demonstrated that the reaction of the $[MoFe_3S_4]^{3+}$ cluster **7** with R_3P gives **8** (R = Pr^i, Bu^t) and with Et_3P affords the double-cubane **9**,[20] both having reduced ($[MoFe_3S_4]^{2+}$) cores. The reduction of **7** is accompanied by oxidation of the tertiary phosphine to R_3PS.[20] We anticipated a similar reduction of **2** with Et_3P. However, product **4** contains the initial 2+ core oxidation level.

The structures of single-cubanes **3** and **4** are shown in Figure 2; metric data are summarized in Table 2. Because of the large amount of dimensional information for these and subsequent clusters, reported data are restricted to ranges and mean values of selected bond distances and angles. The structures confirm retention of tridentate binding by the tris(pyrazolyl)hydroborate ligand in the two clusters and full substitution of chloride in the reaction of **2** with Et_3P. The clusters approach idealized C_3 symmetry, with distorted octahedral coordination at the vanadium sites indicated by mean N−V−N and N−V−S angles of 82 and 166°, respectively. Mean values of V−N and V−S bond distances are 0.03−0.04 Å shorter in **3** than in **4.** Similarly, the V−S distance in **3** is marginally shorter than that in **1** (2.336(5)

(23) Zhu, H.-P.; Liu, Q.-T.; Chen, C.-N. *Chinese J. Struct. Chem.* **2001**, *20*, 19−23.

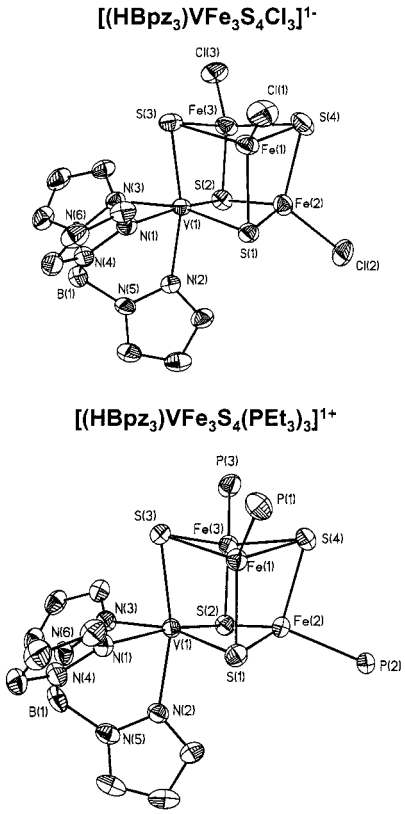

Figure 2. Crystal structures of clusters **3** (top, Me_4N^+ salt) and **4** (bottom, PF_6^- salt) showing 50% probability ellipsoids and atom labeling schemes.

Table 2. Ranges and Mean Values of Selected Bond Distances (Å) and Angles (deg) for Single-Cubanes **3** and **4**

	3	**4**
V−N	2.146(3)−2.166(3) 2.16(1)	2.189(4)−2.192(5) 2.190(2)
V−S	2.303(1)−2.314(1) 2.309(6)	2.346(2) 2.346
Fe−S	2.237(1)−2.265(1) 2.25(1)	2.224(2)−2.241(2) 2.23(1)
V−Fe	2.749(1)−2.779(1) 2.76(2)	2.707(1)−2.734(1) 2.72(1)
Fe−Fe	2.691(1)−2.722(1) 2.71(2)	2.597(1)−2.620(1) 2.61(1)
Fe−Cl/P	2.208(1)−2.219(1) 2.212(6)	2.369(2)−2.392(2) 2.38(1)
N−V−N	81.5−82.5 82.0(5)	80.3(2)−83.2(2) 82(1)
N−V−S	165.1−166.6(1) 165.9(8)	164.7(1)−166.3(1) 165.6(8)

Å)[13] and $[(MeCN)_3VFe_3S_4Cl_3]^{1-}$ (2.332(5) Å),[23] the only other trigonal VFe_3S_4 clusters available for comparison. In other cases, a similar behavior of Mo−S distances occurs, as between the $[MoFe_3S_4]^{3+}$ clusters $[(Cl_4cat)LMoFe_3S_4(SR)_3]^{3-}$ ($L = N_3^-$, CN^-)[19] and $[MoFe_3S_4]^{2+}$ cluster **8**.[20] In several instances, the Mo−S distances are essentially invariant to oxidation state.[20] Evidently, oxidation can involve a core orbital with some heterometal character. However, as will be seen from Mössbauer data, electron distribution at the iron atoms is significantly affected by redox reactions and also by the nature of the terminal ligand.

Reduction of **4** with cobaltocene results in the loss of one phosphine ligand and the formation of the neutral double-cubane **5** (93%), containing $[VFe_3S_4]^{1+}$ cores. This species

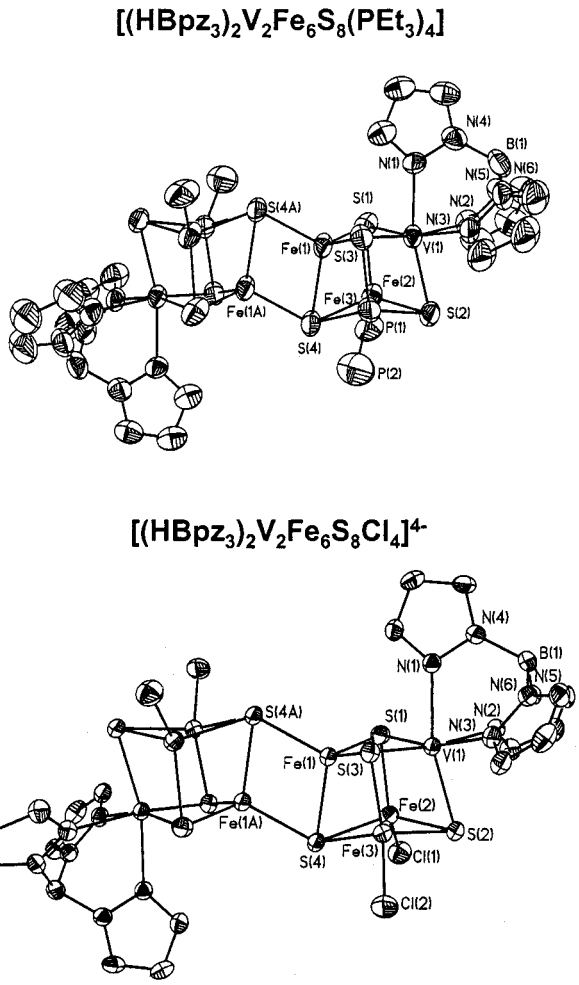

Figure 3. Crystal structures of clusters **5** (top) and **6** (bottom, Et_4N^+ salt) showing 50% probability ellipsoids and atom labeling schemes. Because of disorder, ethyl groups of the Et_3P ligands of **5** are omitted for clarity. Both clusters have crystallographically imposed centrosymmetry.

undergoes phosphine substitution with excess Et_4NCl in acetonitrile to yield the double-cubane tetraanion **6**, isolated as the Et_4N^+ salt (∼60%). Crystallography of **5** and **6** reveals them to be rhomb-bridged double cubanes, shown in Figure 3, with overall structures similar to $[Fe_8S_8(PCy_3)_6]$[24] and $[(Cl_4cat)_2(Et_3P)_2Mo_2Fe_6S_8(PEt_3)_4]^{0,1-}$.[6,20,21] The similarity extends to the irregular and unusual stereochemistry at μ_4−S(4,4A) with Fe−S−Fe bond angles of 66.9−70.5°. The two clusters have imposed inversion centers and closely approach C_{2h} symmetry. Metric parameters are summarized in Table 3. The structures of the individual cubanes are quite similar to those of single-cubanes **3** and **4**, but with a tendency toward slightly longer V−S bonds and a notable distortion arising from bridge formation. The clusters are bridged by the rhombs Fe(1,1A)S(4,4A) with internal angles of ca. 70 and 110° and Fe−S distances significantly *shorter* than intracubane (bridging) Fe−S distances. In **5**, for example, the intercubane bond length Fe(1)−μ_4S(4A) is 0.12 Å shorter than the intracubane distance Fe(1)−μ_4S(4). The latter is 0.06 Å longer than the distances Fe(2,3)−μ_4S(4), which are ca.

(24) Goh, C.; Segal, B. M.; Huang, J.; Long, J. R.; Holm, R. H. *J. Am. Chem. Soc.* **1996**, *118*, 11844−11853.

Table 3. Ranges and Mean Values of Selected Bond Distances (Å) and Angles (deg) for Double-Cubane Clusters **5** and **6**

	5	**6**
V−N	2.175(6)−2.203(7)	2.197(3)−2.205(3)
	2.19(1)	2.200(4)
V−S	2.346(2)−2.387(2)	2.371(1)−2.375(1)
	2.36(2)	2.372(2)
Fe(1)−S(4)[a]	2.394(3)	2.376(1)
Fe(1)−S(4A)[a]	2.270(2)	2.298(1)
Fe(2)−S(4)	2.335(3)	2.391(1)
Fe(3)−S(4)	2.337(3)	2.357(1)
Fe−S[b]	2.231(2)−2.257(3)	2.255(1)−2.284(1)
	2.241(9)	2.27(1)
V−Fe	2.702(2)−2.724(2)	2.763(1)−2.808(1)
	2.71(1)	2.78(2)
Fe(1)−Fe(1A)[a]	2.692(2)	2.649(1)
Fe−Fe[c]	2.606(2)−2.643(2)	2.608(1)−2.748(1)
	2.62(2)	2.696(1)
Fe−Cl/P	2.344(4)−2.366(3)	2.293(1)−2.311(1)
	2.36(2)	2.30(1)
N−V−N	80.1(3)−82.2(3)	80.5(1)−81.3(1)
	81(1)	80.9(3)
N−V−S	163.8(2)−166.2(2)	164.7(1)−165.1(1)
	165(1)	164.9(2)
S(4)−Fe(1)−S(4A)[a]	109.54(8)	110.97(3)
Fe(1)−S(4)−Fe(1A)[a]	70.46(8)	69.03(3)

[a] Bridge rhomb. [b] Remainder of VFe_3S_4 unit. [c] VFe_3S_4 unit.

0.10 Å longer than the Fe−μ_3S bonds within the cubanes. Consequently, all distances do not follow the usual order Fe−μ_4S > Fe−μ_3S found in other clusters such as $[Fe_6S_9(SEt)_2]^{4-}$[25] and $[(edt)_2Mo_2Fe_4S_9]^{3-,4-}$.[26,27] We are unsure of the reason for the shorter rhomb bond distance, but note that the same pattern of distances occurs in the aforementioned rhomb-bridged double cubanes. While two isomers are possible for rhomb-bridged clusters with the core $M_2Fe_6S_8$, all such species place the heterometal in transoid positions.

The reactions in Figure 1 have afforded additional clusters in the $[VFe_3S_4]^{2+}$ oxidation state encountered in the first synthesis of VFe_3S_4 clusters,[12] the second example of a $[VFe_3S_4]^{3+}$ single cubane, and the first isolated $[VFe_3S_4]^{1+}$ clusters, obtained here as rhomb-bridged double cubanes. The latter are effectively isostructural with **9**, containing isoelectronic $[MoFe_3S_4]^{2+}$ cubane units. Compared to their molybdenum analogues, electronic features of VFe_3S_4 clusters[16,28] have been much less thoroughly investigated. We report here some of the essential ground-state electronic features of these molecules.

Electronic Features. Mössbauer spectra, EPR, and magnetic properties have been determined for some or all of clusters **2**−**5** in the solid state. Mössbauer data are provided in Table 4 and spectra in Figures 4, 7, and 9; EPR spectra in Figure 5; and magnetic data in Figures 6 and 8. Isomer shifts from the literature are corrected by 0.12 mm/s when necessary to reference them to iron metal at room temperature.

Table 4. Zero-Field Mössbauer Parameters of Clusters **2**−**5** at 80 K

	mm/s			
cluster	$\delta^{a,b}$	$\Delta E_Q{}^a$	Γ^c	rel intensity[d]
2	0.65	1.15	0.44	1
	0.50	1.10	0.44	2
3[e]	0.43 (0.43)	1.19 (1.17)	0.32 (0.35)	−
4	0.38	1.02	0.32	−
5	0.49	1.32	0.39	1
	0.51	0.90	0.39	2

[a] Typical error ±0.02 mm/s. [b] Relative to Fe metal at ambient temperature. [c] Lorentzian line width, full width at half-maximum. [d] Relative intensity of subspectra. [e] Values at 4.2 K in parentheses.

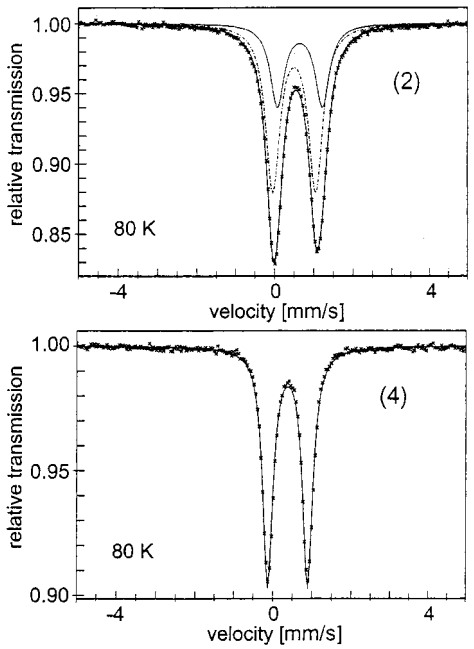

Figure 4. Zero-field Mössbauer spectra of polycrystalline $(Me_4N)_2$[**2**] (top) and [**4**](PF_6) (bottom) at 80 K. Dashed and solid lines are fits to the data using the parameters of Table 4.

(a) $[(HBpz_3)VFe_3S_4Cl_3]^{2-}$. Cluster **2** in the solid state afforded a Mössbauer spectrum that could be deconvoluted into two overlapping quadrupole doublets, which were fitted to a constrained 2:1 intensity ratio and equal line widths (Figure 4). The mean weighted isomer shift of 0.55 mm/s is indistinguishable from that of **1** (0.56 mm/s),[28] indicating that the terminal vanadium ligands $(HBpz_3)^{1-}$ and DMF have no differentiating influence on the electron density at the iron sites, whose isomer shifts are much more sensitive to the terminal ligand.

The EPR spectrum of **2** shows a prominent peak at $g = 5-6$ and a broad signal centered at $g \approx 2$ (Figure 5). The multiline feature in the $g = 2$ region arises from an impurity corresponding to a few percent of the sample (note integrated spectrum) with $S = 1/2$, confirmed by power saturation measurements at 4.2 K. Narrow and broad components exhibit different spin relaxation behavior (not shown). We have no evidence that the $S = 1/2$ signal arises from the $[VFe_3S_4]^{2+}$ core in a spin-doublet state as part of a physical

(25) Hagen, K. S.; Watson, A. D.; Holm, R. H. *J. Am. Chem. Soc.* **1983**, *105*, 3905−3913.
(26) Zhang, Z.; Fan, Y.; Li, Y.; Niu, S.; Li, S. *Kexue Tongbao* **1987**, *32*, 1405−1409.
(27) Zhou, H.-C.; Su, W.; Achim, C.; Rao, P. V.; Holm, R. H. *Inorg. Chem.*, submitted for publication.
(28) Carney, M. J.; Kovacs, J. A.; Zhang, Y.-P.; Papaefthymiou, G. C.; Spartalian, K.; Frankel, R. B.; Holm, R. H. *Inorg. Chem.* **1987**, *26*, 719−724.

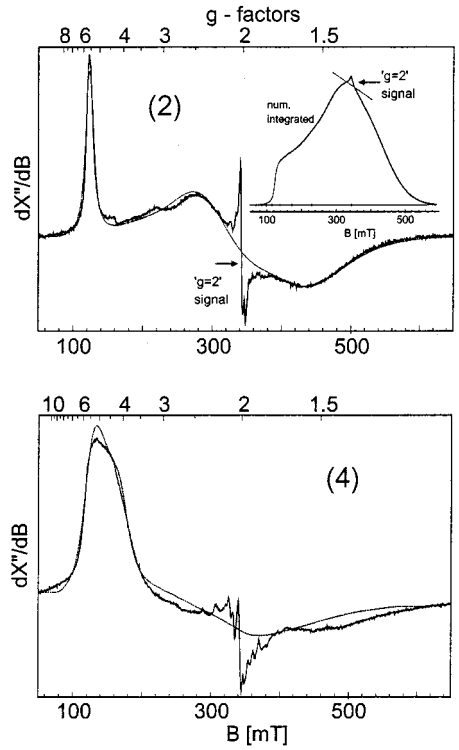

Figure 5. X-Band EPR spectra of **2** and **4** in acetonitrile solutions (1 mM) at 20 K. Top: spectrum of **2** and numerically integrated spectrum (inset) (microwave frequency 9.6336 GHz, power 400 μW, modulation 1.28 mT/100 kHz). The dotted line represents a spin-Hamiltonian simulation with $D = 2.3$ cm^{-1}, $E/D = 0.33$, Lorentzian line shape, line width 70 mT (at $g = 2$, frequency-constant, field-dependent). Bottom: spectrum of **4** (microwave frequency 9.6328 GHz, power 2 mW, modulation 1.28 mT/100 kHz). The dotted line represents a spin-Hamiltonian simulation with $D = 1.11$ cm^{-1}, $E/D = 0.24$, Lorentzian line shape, line width 150 mT (at $g = 2$, frequency-constant, field-dependent). Both spectra contain multiline impurity signals around $g = 2$.

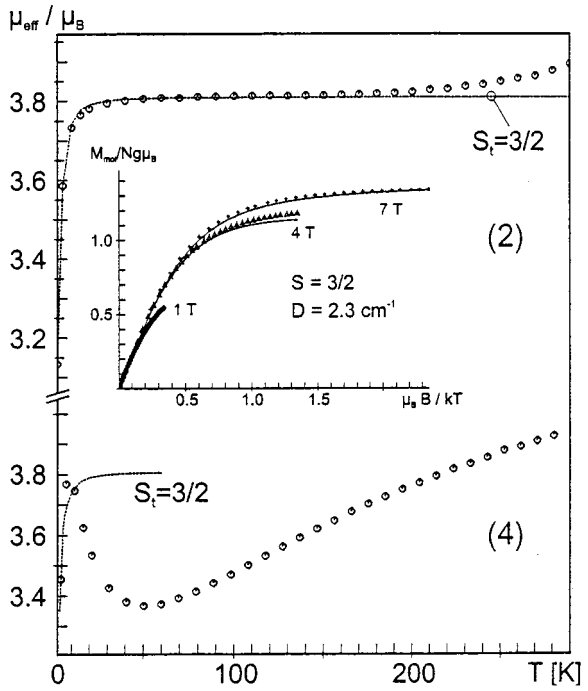

Figure 6. Temperature dependence of the effective magnetic moments of polycrystalline $(Me_4N)_2$[**2**] (top) and [**4**](PF_6) (bottom) (applied field 1 T) and multifield multitemperature measurement of $(Me_4N)_2$[**2**] at 1, 4, and 7 T. The dashed and solid lines are spin-Hamiltonian simulations for $S = 3/2$ with $D = 2.3$ and $E/D = 0.33$ (inset).

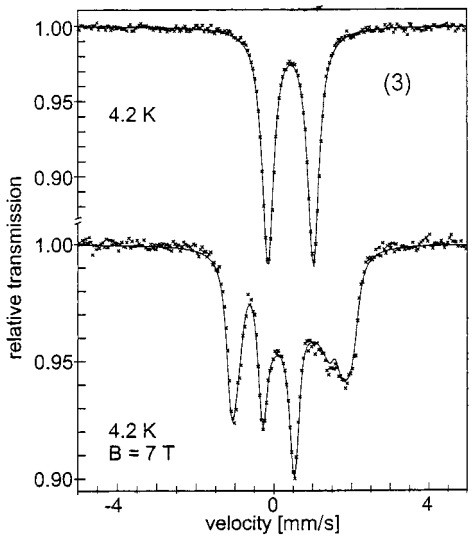

Figure 7. Mössbauer spectra of (Me_4N)[**3**] at 4.2 K in zero field (top) and with a 7 T field applied perpendicular to the γ-rays (bottom). The lower solid line is a simulation for $S = 0$ and $\Delta E_Q = +1.17$ mm/s and asymmetry parameter $\eta = 0.2$.

mixture with an $S = 3/2$ state. The impurity is probably a vanadyl species. The spectrum is indicative of a spin-quartet state with a large rhombic zero-field splitting (ZFS) and could be reasonably well simulated with $S = 3/2$, the axial ZFS parameter $D = 2.3$ cm^{-1} from magnetization measurements (vide infra), and rhombicity $E/D = 0.33$ derived from EPR fits. Simulations showed that the experimental line shape cannot be reproduced with a single set of ZFS parameters. Satisfactory fits were obtained with a Gaussian distribution of E/D values, for which the half-width of the distribution is 0.05. Magnetization measurements on the solid compound confirmed the $S = 3/2$ ground state of **2**. The effective moment of the cluster is constant at $\mu_{eff} = 3.9\mu_B$ at 30−180 K (Figure 6), indicating exclusive population of the spin-quartet ground state in this temperature range. Above 200 K, the magnetic moment increases due to population of excited states with higher spin multiplicities. Below 20 K, the moment decreases due to magnetization saturation by the applied field and the influence of ZFS. The nested magnetization curves are consistent with $S = 3/2$ and $D \neq 0$. These were quantitated by multifield multitemperature measurements and spin-Hamiltonian simulations (inset, Figure 6). With E/D fixed at 1/3 from EPR analysis, the magnetization behavior was satisfactorily fit with $D = 2.3$ cm^{-1}. When these data are taken together with results for three other clusters,[28] it is evident that for the $[VFe_3S_4]^{2+}$ oxidation level, the $S = 3/2$ ground state holds over (at least) three sets of terminal ligands at the vanadium site and with chloride and thiolate terminal ligands at the iron sites.

(b) $[(HBpz_3)VFe_3S_4Cl_3]^{1-}$. The Mössbauer spectrum of cluster **3** in the solid state consists of a symmetric quadrupole doublet (Figure 7). In the range of 2−120 K, $\mu_{eff} \lesssim 0.3\mu_B$, indicating an $S = 0$ ground state (Figure 8). The weak paramagnetic moment of the sample below ca. 120 K arises from an impurity that, if an Fe(III) monomer with a

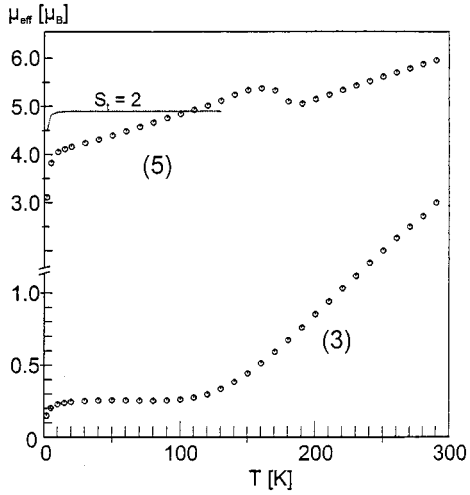

Figure 8. Temperature dependence of the effective magnetic moments of polycrystalline **5** (top) and (Me_4N)[**3**] (bottom) (applied field 1 T). The dashed line represents a spin-Hamiltonian simulation for $S = 2$ with $D = E/D = 0$.

molecular weight similar to the cluster is adopted, is a ca. 0.02 mol fraction of the sample. The significant increase in the effective moment above 150 K indicates thermal population of excited spin states with higher multiplicities. A diamagnetic ground state is corroborated by the Mössbauer spectrum in an applied field of 7 T (Figure 7), which demonstrates the absence of an internal magnetic field. The magnetically perturbed spectrum could also be simulated with indistinguishable iron sites. The isomer shift of **3** (0.43 mm/s) is substantially lower than the mean value of **2**, indicating a more oxidized set of iron atoms. It is comparable to the value (0.37 mm/s) for the double-cubane $[V_2Fe_6S_8(SEt)_9]^{3-}$,[16] which, however, has terminal thiolate ligands that in general tend to decrease isomer shifts relative to chloride. The double cubane is also diamagnetic and together with **3** indicates that the intrinsic ground state of the $[VFe_3S_4]^{3+}$ core with tetrahedrally coordinated iron atoms is $S = 0$. Magnetic data down to 24 K for $[VFe_3S_4(Et_2dtc)_4]^{1-}$, which has five-coordinate iron sites,[17] do not establish the ground-state spin of this cluster, the third known example of the $[VFe_3S_4]^{3+}$ oxidation state.

(c) $[(HBpz_3)VFe_3S_4(PEt_3)_3]^{1+}$. Cluster **4** as its polycrystalline PF_6^- salt exhibits a sharp symmetric quadrupole doublet in its Mössbauer spectrum (Figure 4). Its isomer shift of 0.38 mm/s is 0.17 mm/s less than that of isoelectronic, chloride-ligated **2**, a behavior consistent with previous observations that substitution of chloride or thiolate with tertiary phosphine in isoelectronic clusters decreases the isomer shift.[20,24,29,30]

Interpretation of the EPR spectrum of **4** (Figure 5) is less straightforward than for **2** because of its somewhat unusual shape, which is similar to the spectra of certain synthetic[30] and protein-bound[31] $[Fe_4S_4]^{1+}$ clusters with an $S = 3/2$ ground state. For the latter cluster, in a bacterial dehydratase, the EPR simulation traced the spectral shape back to a rather simple distribution of E/D similar to the situation with **2**. Using the same approach, a reasonably good simulation was obtained. The optimized parameters are $D = 1.11$ cm^{-1} and a Gaussian distribution of E/D values with a mean $E/D = 0.24$ and a half-width of 0.13. In contrast to biological systems where protein structure may inflict "strain" upon ZF parameters from microheterogeneity of the cluster environment, a similar effect in well-defined synthetic clusters such as **4** may indicate an inherent "plasticity" of structure. This property is manifested by numerous different core distortions of $[Fe_4S_4(SR)_4]^{3-}$ clusters from T_d symmetry in the crystalline state.[32,33]

The temperature dependence of the effective magnetic moment of **4** is more complex than that of isoelectronic **2** (Figure 6). Above ca. 10 K, the data closely approach the spin-only value for $S = 3/2$ ($3.87\mu_B$) and demonstrate a spin-quartet ground state. The dotted line is an approximate spin-Hamiltonian simulation calculated for $S = 3/2$ with the ZFS parameters from EPR. The up−down variation of the moment with temperature and the occurrence of a minimum, at about 50 K, are typical of a spin ladder with one (or more) $S = 1/2$ states close to the ground state and higher spin states at higher energies. Hence, the spin coupling schemes of **2** and **4** are considerably different.[34]

(d) $[(HBpz_3)_2V_2Fe_6S_8(PEt_3)_4]$. The Mössbauer spectrum of polycrystalline double-cubane **5** consists of a broadened quadrupole doublet at 80 K and two subspectra at 4.2 K (Figure 9). Both spectra were fitted with two quadrupole doublets having a constrained 2:1 intensity ratio at 80 K and an unconstrained 2.1:1 ratio at 4.2 K. The spectra are consistent with the structure of centrosymmetric **5** (Figure 3), which has a 2:1 population of iron atoms. The mean isomer shift is 0.50 mm/s, 0.12 mm/s larger than that for **4** and signifying reduction to a species containing two $[VFe_3S_4]^{1+}$ units. The cluster is paramagnetic over the entire 2−300 K interval (Figure 8). At 10 K, the effective moment is slightly higher than $3.9\mu_B$ and increases monotonically up to ca. $6\mu_B$ at 300 K, except for an irregularity centered near 170 K. It is difficult to imagine a particular coupling scheme with an unusual spin ladder that would generate such an effect at 170 K within a narrow temperature interval of less than 30 K. We tentatively ascribe this behavior to a phase transition. Other than high-spin Fe(III) impurity signals and a weak unidentified feature at $g \approx 2$, the X-band EPR spectra of preparations of **5** in acetonitrile solution are silent, indicative of an integer-spin ground state. The ground-state spin cannot be determined with the data at hand. Because the low-temperature moment is less than that for an isolated $S = 2$ state ($4.9\mu_B$, Figure 8), we surmise that the ground state may

(29) Carney, M. J.; Papaefthymiou, G. C.; Whitener, M. A.; Spartalian, K.; Frankel, R. B.; Holm, R. H. *Inorg. Chem.* **1988**, *27*, 346−352.
(30) Carney, M. J.; Papaefthymiou, G. C.; Spartalian, K.; Frankel, R. B.; Holm, R. H. *J. Am. Chem. Soc.* **1988**, *110*, 6084−6095.
(31) Hans, M.; Buckel, W.; Bill, E. *Eur. J. Inorg. Chem.* **2000**, *267*, 7082−7093.
(32) Carney, M. J.; Papaefthymiou, G. C.; Frankel, R. B.; Holm, R. H. *Inorg. Chem.* **1989**, *28*, 1497−1503.
(33) Excoffon, P.; Laugier, J.; Lamotte, B. *Inorg. Chem.* **1991**, *30*, 3075−3081.
(34) Because in the above situation multiplets of different total spin can be mixed under the influence of a single-ion ZFS, the parameters derived from the EPR simulation should be taken with some care and might not necessarily describe the intrinsic properties of the ground-state spin-quartet.

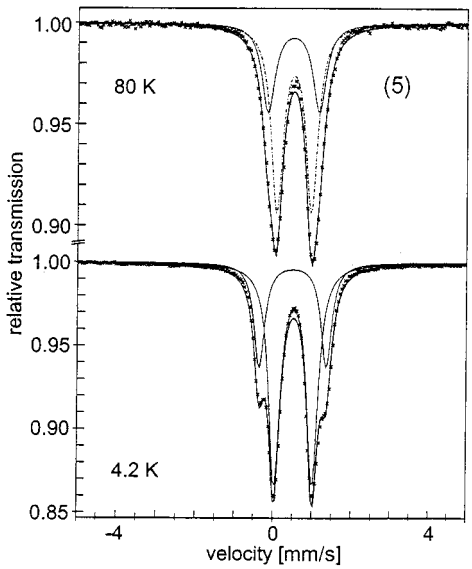

Figure 9. Zero-field Mössbauer spectra of **5** at 80 K (top) and 4.2 K (bottom). Dashed and solid lines are fits to the data using the parameters of Table 4.

be a quantum mechanical mixture of close-lying states of differing spin multiplicities with dominant $S = 2$ character.

Electron Distribution and Oxidation States. A property of considerable interest since the discovery of heterometal cubane-type clusters is the distribution of electrons over the core metal atoms and the attendant matter of oxidation state assignment.[35] This problem has been approached by analysis of ^{57}Fe isomer shifts, which reflect the charge density at the nucleus and depend critically on the population of the 3d valence orbitals. For tetrahedral $FeS_{4-n}(SR)_n$ units, separate clusters or part of a cluster with the metal in the (mean) oxidation state *s*, isomer shifts vs iron metal at 4.2 K have been fitted to the linear relationship $\delta = 1.36-0.36s$.[16] The relationship has been derived from a database encompassing the oxidation states $Fe^{2+,3+}$ and intermediate values and predicts that the isomer shift per iron atom varies by -0.36 mm/s upon one-electron oxidation.[36] Typically, for iron−sulfur clusters there is very little difference ($\leq$0.02 mm/s) between isomer shifts at 4.2 and 77−80 K. Deduction of *s* allows estimation of the heterometal atom valence state by difference if the core charge is known. No comparable databases exist for FeS_3L units with $L = Cl^-$ and PR_3. A possible caveat to the procedure is that the heterometal, by virtue of a different charge and valence electrons with different energy and spin, may perturb spin-dependent charge delocalization in the core. This point was recognized at the outset,[37,38] but its effect is likely to be small. With no experimental approach evidently being superior, we proceeded with the empirical correlation between isomer shift and oxidation state assuming that variation of one ligand out of four does not appreciably affect the 0.12 mm/s shift for a one-electron change per three iron atoms.

The isomer shift difference of FeS_3Cl sites in **2** and **3**, $\delta_{av}(\mathbf{3}) - \delta(\mathbf{2}) = -0.12$ mm/s, is the same as the predicted difference for removal of one delocalized electron per three iron atoms, i.e., $-0.36/3 = -0.12$ mm/s. Thus, these clusters are related by a largely Fe_3 subcluster-based redox event and the vanadium atoms are in the same oxidation state. By using the empirical relationship, isomer shift reference values can be estimated for subclusters of $[VFe_3S_4]^z$ cores sharing integral numbers of valence electrons. A useful reference species for further interpretation of Mössbauer data is $[Fe_4S_4Cl_4]^{2-}$, a delocalized cluster with oxidation state $Fe^{2.5+}$ and isomer shift $\delta = 0.51$ mm/s at 77 K. We estimate $\delta = 0.33$ mm/s (0.51−0.36/2) for the hypothetical $Fe^{3+}{}_3$ subcluster of the $[Fe_4S_4]^{3+}$ core. Because the vanadium atom does not appear to participate significantly in the redox step that links **2** and **3**, it is reasonable to estimate isomer shifts for Fe_3 subclusters reduced by one and two electrons. We obtain $\delta = 0.45$ mm/s for $Fe^{3+}{}_2Fe^{2+}$ and $\delta = 0.57$ mm/s for $Fe^{3+}Fe^{2+}{}_2$ by adding increments of $0.36/3 = 0.12$ mm/s per one electron over the three sites. The shifts of **3** (0.43 mm/s) and **2** (0.55 mm/s) differ from the value for the $Fe^{3+}{}_3$ subcluster but are close to the values for the $Fe^{3+}{}_2Fe^{2+}$ and $Fe^{3+}Fe^{2+}{}_2$ motifs, respectively. We conclude that **2** is described by $[V^{3+}Fe^{3+}Fe^{2+}{}_2S_4]^{2+}$ and **3** by $[V^{3+}Fe^{3+}{}_2Fe^{2+}S_4]^{3+}$. When the same procedure is applied to the previously reported clusters **1** ($\delta = 0.56$ mm/s) and $[(Me_2PCH_2CH_2PMe_2)(MeCN)VFe_3S_4Cl_3]^{1-}$ ($\delta_{av} = 0.54$ mm/s) with the indicated isomer shifts at 80 K,[28] the core description of **2** emerges.

As already noted, the isomer shift of the phosphine-ligated cluster **4** (0.38 mm/s) is significantly lower than that of chloride-ligated cluster **2** with an isoelectronic $[VFe_3S_4]^{2+}$ core. Because tertiary phosphine ligands induce lower isomer shifts than chloride or thiolate in isoelectronic Fe_4S_4 and MFe_3S_4 clusters, the species $[Fe_4S_4(PR_3)_4]^{1+}$ (R = Cy, Pr^i, Bu^t) are the best available references for the $[Fe_4S_4]^{1+}$ core ($Fe^{2.25+}$). Their isomer shifts are, however, somewhat dependent on the R substituent: Pr^i, 0.46 mm/s; Cy, 0.48 mm/s; Bu^t, 0.51 mm/s (77 K).[24,39] The above procedure gives $\delta = 0.28-0.31$ mm/s for the $Fe^{3+}{}_2Fe^{2+}$ subcluster and $\delta = 0.40-0.43$ mm/s for the $Fe^{3+}Fe^{2+}{}_2$ subcluster, suggesting the $[V^{3+}Fe^{3+}Fe^{2+}{}_2S_4]^{2+}$ description for **4**. Application of the same procedure for the thiolate cluster $[(DMF)_3VFe_3S_4(SC_6H_4\text{-}p\text{-}Me)_3]^{1-}$ ($\delta = 0.46$ mm/s)[28] with $[Fe_4S_4(SPh)_4]^{2-}$ ($\delta = 0.46$ mm/s)[40] is not decisive between $[V^{3+}Fe^{3+}{}_2Fe^{2+}S_4]^{2+}$ (0.40 mm/s) and $[V^{3+}Fe^{3+}Fe^{2+}{}_2S_4]^{3+}$ (0.52 mm/s), whose Fe_3 isomer shifts are indicated. If the full range of isomer shifts reported for $[Fe_4S_4(SR)_4]^{2-}$ clusters at 77 K (0.43−0.47 mm/s, R = alkyl, aryl)[40−43] is used, the conclusion is unchanged.

(35) Holm, R. H. *Chem. Soc. Rev.* **1981**, *10*, 455−490.
(36) A linear relationship between oxidation state and isomer shift (relative to iron metal at 4.2 K), based on a less extensive database and with similar numerical parameters, was reported in the early development of heterometal cubane clusters.[35,37,38]
(37) Christou, G.; Mascharak, P. K.; Armstrong, W. H.; Papaefthymiou, G. C.; Frankel, R. B.; Holm, R. H. *J. Am. Chem. Soc.* **1982**, *104*, 2820−2831.
(38) Mascharak, P. K.; Papaefthymiou, G. C.; Armstrong, W. H.; Foner, S.; Frankel, R. B.; Holm, R. H. *Inorg. Chem.* **1983**, *22*, 2851−2858.
(39) A better reference would be $[Fe_4S_4(PEt_3)_4]^{1+,2+}$. However, in all attempts thus far, PEt_3 forms the "basket" clusters $[Fe_6S_6(PEt_3)_4L_2]$ ($L = Cl^-$,[44] RS^-[45]) rather than cubanes.
(40) Frankel, R. B.; Averill, B. A.; Holm, R. H. *J. Phys. (Paris)* **1974**, *36(C5)*, 107−111.
(41) Barclay, J. E.; Evans, D. J.; Leigh, G. J.; Newton, M. S.; Silver, J. *Gazz. Chim. Ital.* **1994**, *124*, 367−370.

However, for the double-cubane $[V_2Fe_6S_8(SEt)_9]^{3-}$ ($\delta = 0.37$ mm/s),[16] the $[V^{3+}Fe^{3+}{}_2Fe^{2+}S_4]^{3+}$ description is indicated.[16,28]

Because the preceding treatment is entirely empirical and depends on small differences in isomer shifts, we do not insist upon the formalistic core oxidation descriptions but offer them as the best current approximations to electron distribution in these delocalized species. Certainly, descriptions such as $[V^{1+}Fe^{3+}{}_3S_4]^{2+}$, $[V^{2+}Fe^{3+}{}_3S_4]^{3+}$, and $[V^{4+}Fe^{2+}{}_3S_4]^{2+}$ are not valid. The isomer shifts *require* mixed-valence iron cores. Earlier analyses based on collective structural and (less extensive) isomer shift data for two $[VFe_3S_4]^{2+}$ thiolate-ligated clusters favored a mean iron oxidation state just above 2.5+.[16,28] At least in the chloride-ligated cubanes, the V^{3+} ion is a surrogate for Fe^{3+} in a homometallic cubane but with significantly less participation in the electron delocalization aspect. Our previous analysis of charge distribution involved direct comparison of isomer shifts. The present procedure is based on the empirical correlation and reference shifts from $[Fe_4S_4]^{2+,1+}$ clusters with the appropriate ligation and thus approximates the charge effect of the heterometal atom.

Summary. The following are the principal results and conclusions of this investigation.

(1) Cubane-type cluster **2**, readily obtained from **1** by a ligand substitution reaction at the vanadium site,[14] possesses an $S = 3/2$ ground-state found earlier for $[VFe_3S_4]^{2+}$ clusters with different ligation patterns at the vanadium and iron sites[28] and for isoelectronic $[MoFe_3S_4]^{3+}$ clusters.[38] The implication from the collective results on clusters of both types is that the spin-quartet ground state is a general property.

(2) Cluster **2** is a precursor to other cubane-type VFe_3S_4 clusters (Figure 1). Reaction with ferrocenium ion affords the $[VFe_3S_4]^{3+}$ cluster **3** with an $S = 0$ ground state. Reaction with PEt_3 does not result in core reduction as with $[MoFe_3S_4]^{3+}$ clusters[20] but proceeds with ligand substitution to yield $[VFe_3S_4]^{2+}$ cluster **4**. Reaction of **4** with cobaltocene results in reduction and formation of edge-bridged double-cubane **5**, whose $[V_2Fe_6S_8]^{2+}$ core is isostructural with molybdenum cluster **9**[20,21] and its monoanion.[6]

(3) ^{57}Fe isomer shifts of isoelectronic cubane-type clusters $[L'MFe_3S_4L_3]^z$ decrease in the order $L = Cl^- > RS^- > R_3P$.

(4) Analysis of isomer shifts based on an empirical correlation between shift and oxidation state and appropriate reference shifts results in two conclusions. (i) The oxidation $\mathbf{2} \rightarrow \mathbf{3} + e^-$ results in a change in electron density localized largely or completely on the Fe_3 subcluster and associated sulfur atoms. (ii) The most appropriate charge distributions are $[V^{3+}Fe^{3+}Fe^{2+}{}_2S_4]^{2+}$ ($Fe^{2.33+}$) for **1**, **2**, and **4** and $[V^{3+}Fe^{3+}{}_2Fe^{2+}S_4]^{3+}$ ($Fe^{2.67+}$) for **3** and $[V_2Fe_6S_8(SEt)_9]^{3-}$. Conclusion i applies to every MFe_3S_4 cubane-type cluster thus far examined in different redox states at parity of cluster ligation.[37,38] Conclusion ii carries the intuitively satisfying result that the constant oxidation state of heteroatom M is common, i.e, V^{3+} or $Mo^{3+,4+}$.[20,28,37,38]

This work completes the first stage of our renewed investigation of VFe_3S_4 clusters. It remains to be seen if one or more of these clusters provides a synthetic entry to species resembling the clusters of nitrogenase, as is the case for molybdenum cluster **9**, which, as noted at the beginning, leads to structures that are topological analogues of the nitrogenase P^N clusters.[5,6]

Acknowledgment. This research was supported by NIH Grant GM 28856. C.H. is grateful to the Deutscher Akademischer Austauschdienst (DAAD) for a postdoctoral fellowship.

Supporting Information Available: X-ray crystallographic files in CIF format for the structure determinations of the four compounds in Table 1. This material is available free of charge via the Internet at http://pubs.acs.org.

IC011011B

(42) Barclay, J. E.; Davies, S. C.; Evans, D. J.; Hughes, D. L.; Longhurst, S. *Inorg. Chim. Acta* **1999**, *291*, 101−108.
(43) Silver, J.; Fern, G. R.; Miller, J. R.; McCammon, C. A.; Evans, D. J.; Leigh, G. J. *Inorg. Chem.* **1999**, *38*, 4256−4261.
(44) Snyder, B. S.; Holm, R. H. *Inorg. Chem.* **1988**, *27*, 2339−2347.
(45) Reynolds, M. S.; Holm, R. H. *Inorg. Chem.* **1988**, *27*, 4494−4499.